Multi-wavelength observations of Mrk 501 in 2008

D. Kranich[*], A. Falcone[†], M. Giroletti[‡], T. Hovatta[§], Y.Y. Kovalev[¶], A. Lahteenmaki[§], E. Nieppola[§], C. Pagani[†], D. Paneque[‖], A. Pichel[**], K. Satalecka[††], J. Scargle[xiii], D. Steele[‡‡], F. Tavecchio[x], D. Tescaro[xi], M. Tornikoski[§] and M. Villata[xii]
on behalf of GASP-WEBT, MAGIC, VERITAS

[*] *ETH Zurich, CH-8093 Switzerland*
[†] *Penn State University, Astronomy & Astrophysics Dept., University Park, PA 16802, USA*
[‡] *INAF Istituto di Radioastronomia, Bologna, Italy*
[§] *Metsahovi Radio Observatory, Helsinki University of Technology TKK, Finland*
[¶] *MPIfR, Bonn, Germany and ASC Lebedev, Moscow, Russia*
[‖] *SLAC National Accelerator Laboratory and KIPAC, CA 94025, USA*
[**] *Institute de Astronomia y Fisica del Espacio Ciudad Universitaria, Buenos Aires, Argentina*
[††] *DESY Deutsches Elektronen-Synchrotron, D-15738 Zeuthen, Germany*
[‡‡] *Adler Planetarium & Astronomy Museum, 1300 S. Lakeshore Dr., Chicago, IL 60605, USA*
[x] *INAF National Institute for Astrophysics, I-00136 Rome, Italy*
[xi] *IFAE, Edifici Cn., Campus UAB, E-08193 Bellaterra, Spain*
[xii] *INAF Osservatorio Astronomico di Torino, Italy*
[xii] *SLAC, USA*

Abstract. **The well-studied VHE ($E > 100$ GeV) blazar Mrk 501 was observed between March and May 2008 as part of an extensive multi-wavelength observation campaign including radio, optical, X-ray and VHE gamma-ray instruments. Mrk 501 was in a low state of activity during the campaign, with a VHE flux of about 20% the Crab Nebula flux. Despite the modest flux level significant flux variations could be observed in X-rays. Strong variations were also seen in γ-rays although obscured by large measurement errors. Overall Mrk 501 showed an increased variability when going from radio to γ-ray energies. The broad band SED during the two different emission states of the campaign was well described by a homogeneous one-zone SSC model. The best-fit results were obtained using a magnetic field strength $B = 0.19$ G, a Doppler factor $\delta = 12$ and a broken power-law electron spectrum with slopes $n_1 = 2.0$ and $n_2 = 4.2$ for the low and $n_2 = 3.6$ for the high state respectively. Besides the electron spectrum slope, the break energy γ_{break} also had to be adjusted in order to fit the low ($\gamma_{break} = 2.2 \cdot 10^5$) and high ($\gamma_{break} = 2.6 \cdot 10^5$) emission states.**

Keywords**: Blazar, Mrk 501, SSC-model**

I. Introduction

Mrk 501 is a well known nearby (redshift z=0.034) blazar which was first detected at TeV energies by the Whipple collaboration in 1996 [1]. In subsequent years Mrk 501 was regularly observed and detected at VHE γ-rays by many other Cherenkov telescope experiments. In particular during 1997 when it showed an exceptionally strong outburst with peak flux levels up to 10 times the Crab Nebula flux and flux doubling time scales down to 0.5 days [2]. Mrk 501 also showed strong flaring activity at X-ray energies during that time. The obtained X-ray spectrum was very hard and the synchrotron peak was found to be at ~ 100 keV, about 2 orders of magnitude higher than in previous observations [3]. In the following years Mrk 501 only showed a low γ-ray emission at the order of 20-30% the Crab Nebula flux together with a few single flares of higher intensity. In 2005, the MAGIC telescope was able to observe Mrk 501 during another high emission state which, although at a lower flux level compared to 1997, showed flux variations by an order of magnitude and unprecedented flux doubling time scales down to a few minutes [4]. Mrk 501 was target of many multi-wavelenght (MWL) campaigns (e.g. [5], [6], [7], [8]) mainly covering the object during a flaring activity. The data presented here were taken between March 25th and May 16th, 2008 during an extended MWL campaign covering radio (EFfelsbert, IRAM, Medicina, Metsahovi, Noto, RATAN-600, VLBA), optical (GASP/KVA), UV (Swift/UVOT), X-ray (RXTE/PCA, Swift/XRT) and γ-ray (MAGIC, Whipple, VERITAS) energies. The duration as well as energy coverage of this particular Mrk 501 campaign is rather unique.

II. Light Curves

Figure 1 shows the normalized light curves[1] for a selection of the instruments involved in the campaign. The different light curves cover the optical R band (GASP/KVA), the UV band (Swift/UVOT), the X-ray band (RXTE/PCA) and the VHE band (MAGIC and VERITAS). The average flux values in the different energy bands are given as: 3.8? mJy (GASP / KVA),

[1] Each individual light curve was normalized onto its average

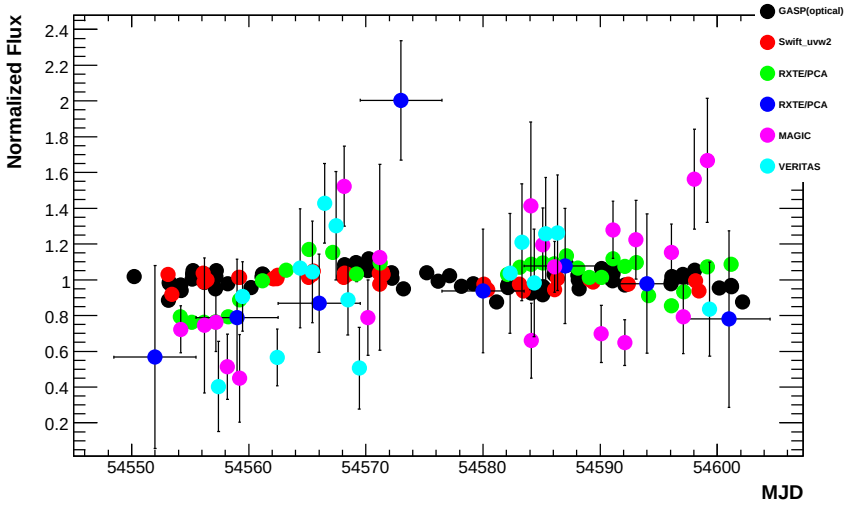

Fig. 1: Combined normalized lightcurves for a selection of the instruments taking part in the campaign. Only statistical errors are shown.

3.4? mCrab (RXTE/PCA), xxx (Swift/UVOT) and 20% the Crab nebula flux (MAGIC and VERITAS). Other instruments providing valuable data (like Swift/XRT or Whipple) have been omitted for the sake of clarity in this plot. As can be seen, flux variations are large at X-rays and γ-rays, but rather small at UV and in the optical. Due to the small error bars in the X-ray data, the most significant flux variations could be observed at these energies. The plot also shows some evidence for a correlated flux variability at X-rays and VHE γ-rays indicating a low emission state between MJD 54550 and 54560 and a somewhat stronger emission during MJD 54560-54574 and MJD 54574-54602, the latter two regions only separated by the data gap at most frequencies. These three regions were also used separately as part of the SED analysis presented below. Variability patterns will be discussed in the following two sections.

III. VARIABILITY

We followed the description given in [9] to quantify the flux variability by means of the so-called fractional variability parameter F_{var}. In order to account for the individual flux measurement errors ($\sigma_{err,i}$) the 'excess variance' ([10], [11]) as an estimator of the intrinsic source flux variance. This is the variance after subtracting the expected contribution from measurement errors. F_{var} was derived for each individual instrument taking part in the campaign which covered an energy range from radio frequencies at $\sim$8 GHz up to very high energies at $\sim$10 TeV. F_{var} is calculated as:

$$F_{var} = \sqrt{\frac{S^2 - < \sigma_{err}^2 >}{< F_\gamma >^2}} \qquad (1)$$

Here $< F_\gamma >$ denotes the average photon flux, S the standard deviation of the N flux measurements and $< \sigma_{err}^2 >$ the average mean squared error, all determined for a given instrument (energy bin). The uncertainty on F_{var} is estimated according to:

$$\Delta F_{var} = \frac{< \sigma_{err}^2 >}{\sqrt{N} < F_\gamma >} \cdot \sqrt{1 + \frac{1}{2 < F_\gamma >^2 F_{var}^2}} \qquad (2)$$

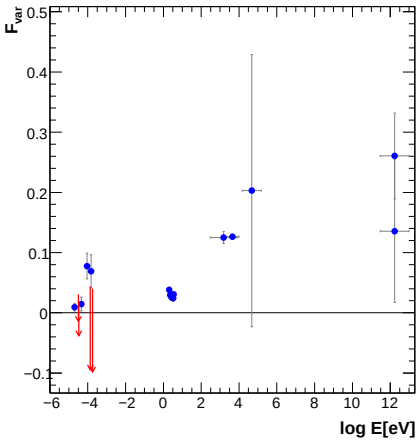

Fig. 2: Fractional variability parameter F_{var} as derived according to [9] for all the instruments that participated in the campaign. F_{var} was computed using the measured fluxes from the individual single night observations except for Swift / BAT for which data integrated over one week was used. Vertical bars denote 1 σ uncertainties, horizontal bars indicate the approximate energy range covered by the instrument. The red arrows indicate 95% confidence level upper limits.

Fig. 2 shows the derived F_{var} values for all instruments that participated in the MWL campaign. Note that several instruments show a negative F_{var}, even though the vertical error bars are large and almost reach

positive F_{var} values. These points are due to a negative excess variance where $< \sigma_{err}^2 >$ is larger than S^2. This can happen when there is little variability and/or the individual flux errors are slightly overestimated. In order to avoid imaginary numbers in those cases we take the negative excess variance in eq. 1 and give F_{var} a negative sign, too. Essentially such a result can be interpreted as no signature for variability in the data of that particular instrument, either because a) there was no variability or b) the instrument was not sensitive enough to detect it.
The plot, on the other hand, also shows significant variability detected with various other instruments during the campaign. Essentially all instruments observing at optical or larger frequencies recorded variability. The plot also shows some evidence that the recorded flux variability increases with energy: in the optical R band (ground based telescopes) and the 6 filters from Swift/UVOT the variability is around 2-4%, in X-rays it is about 13%, and at VHE at the 20% level, although affected by large error bars (due to the large uncertainties in the flux measurements). The radio instruments show no evidence for variability, with the exception of Metsahovi, that shows 7+/-2 %.

In the Synchrotron Self-Compton (SSC) framework, the observed flux variability contains information on the dynamics of the underlying population of relativistic electrons (and possibly positrons). In this context, the general variability trend reported in Fig. 2 suggests that the flux variations are produced by the injection of energetic particles, that are characterized by shorter cooling timescales; causing the higher variability amplitude observed at the highest energies.

IV. MULTIFREQUENCY CROSS-CORRELATIONS

In order to study the multi-frequency cross correlations between the different energy bands we used the Discrete Correlation Function (DCF) as described in [12]. This method can also be applied in the case of unevenly sampled data as taken in this campaign.
The DCF was derived for all different combinations of instruments / energy regions and, in addition, also for artificially introduced time lags (ranging from -10 to +10 days) between the individual light curves. Such time lags may occur as a result of spatially separated emission regions of the individual flux components, as expected e.g. in External Inverse Compton models, or may be caused by the energy dependent cooling time-scales of the emitting electrons.
Based on the MWL data from this campaign, only significant correlations for the pairs RXTE/PCA - Swift/XRT and also (less significant) RXTE/PCA (or Swit/XRT) with MAGIC (or VERITAS) have been found (Fig. 3a and 3b). In both cases the maximum DCF value is obtained for a zero time lag. Due to the modest flux variability and / or large flux errors no strong conclusions could be drawn from this analysis.

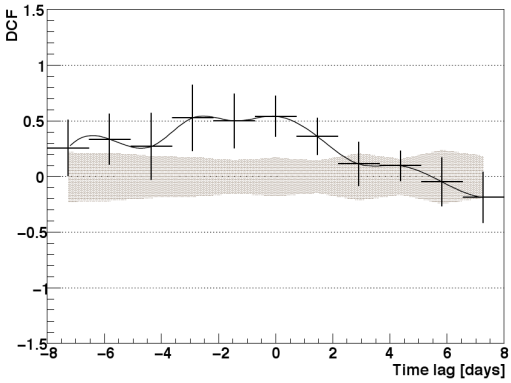

(a) RXTE vs. Magic

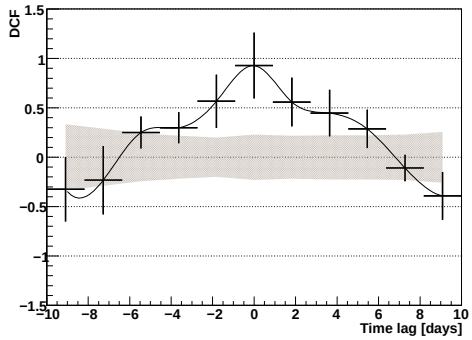

(b) RXTE vs. XRT

Fig. 3: Discrete Correlation Function for time lags spanning from -10 to +10 days in steps of 2 day. The grey band represents the expected fluctuation of the DCF values in the case of completely uncorrelated time series given the error bars from the actual observations.

V. SED MODELLING

TABLE I: The SSC-model parameters used to describe the broad band SED for different flux states of the campaign

	2008 high state	2008 low state	2005 high	2005 low
γ_{break}	$2.6 \cdot 10^5$	$2.2 \cdot 10^5$	$1.0 \cdot 10^6$	$1.0 \cdot 10^5$
n_1	2.0	2.0	2.0	2.0
n_2	3.9	4.2	3.9	3.2?
B [G]	0.19	0.19	0.23	0.31
K [cm^{-3}]	$1.8 \cdot 10^4$	$1.8 \cdot 10^4$	$7.5 \cdot 10^4$	$4.3 \cdot 10^4$
R [cm]	$3 \cdot 10^{15}$	$3 \cdot 10^{15}$	$1 \cdot 10^{15}$	$1 \cdot 10^{15}$
δ	12	12	25	25

The broad band SED of Mrk 501 for the three different time periods defined above, together with some historical data fromt the 2005 low and high state of the object are shown in Fig. 4. The host galaxy contribution (12.0 ± 0.3 mJy [13]) has been subtracted from the optical (KVA) data while the γ-ray spectra have been corrected for EBL absorption using the 'low-IR' model of [14]. The results from a one-zone SSC model fit to the different data sets are also shown in the figure as dashed lines. The model code was developed by

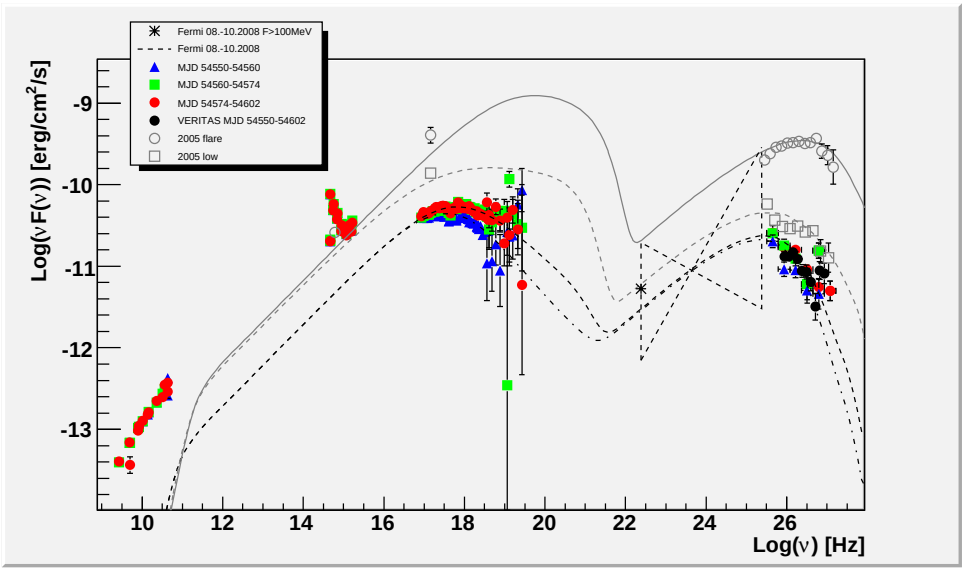

Fig. 4: Broadband SED for Mrk 501 as obtained during this campaign in comparison to a past low and high state from 2005. The results from a SSC model fit to the data are shown as solid and dashed lines.

Tavecchio et al. ([15], [7]) and is based on the following characteristic parameters: a spherically shaped emission region with radius R and Doppler factor δ, a magnetic field of strenght B, an electron distribution (density K) following a broken power law with slopes n_1 and n_2 and break energy γ_{break}. The actual values of these model parameters for the two different emission states during the campaign and the historical data from 2005 are given in table I. As can be seen from Fig. 4 the model is able to accurately reproduce the data at X-ray energies. Given the relatively small differences in the SEDs of the two emission states of the campaign, only marginal changes of the model parameters were required in order to adjust the model to the two states. The proposed explanation for the low - high state transition is the injection of fresh, high energy electrons which lead to a shift of the γ_{break} energy and to a hardening of the spectrum.
The discrepancy between the model and the data at lower energies (radio, optical) can be caused by synchrotron radiation from additional, cooler electron populations located further down the jet. In comparison to the historical 2005 SED the model parameters have changed significantly. We attribute this difference to the sparse energy coverage of the 2005 data which does not allow to constrain the large number of model parameters accurately.

ACKNOWLEDGMENTS

We thank the Instituto de Astrofisica de Canarias for the excellent working conditions at the Observatorio del Roque de los Muchachos in La Palma. The support of the German BMBF and MPG, the Italian INFN and Spanish MCINN is gratefully acknowledged. This work was also supported by ETH Research Grant TH 34/043, by the Polish MNiSzW Grant N N203 390834, and by the YIP of the Helmholtz Gemeinschaft.

REFERENCES

[1] J. Quinn, *et al.* 1996, ApJ, 456, L831
[2] F. Aharonian, *et al.* 1999, A&A, 342, 69
[3] E. Pian, *et al.* 1998, ApJ, 492, L17
[4] J. Albert, *et al.* 2007, ApJ, 669, 862
[5] J. Kataoka, *et al.* 1999, ApJ, 514, 138
[6] H. Krawczynski, *et al.* 2000, A&A, 353, 97
[7] F. Tavecchio, *et al.* 2001, ApJ, 554, 725
[8] H. Anderhub, *et al.* 2009, submitted to ApJ
[9] S. Vaughan, *et al.* 2003, MNRAS, 345, 1271
[10] K. Nandra, *et al.* 1997, ApJ, 476, 70
[11] R. Edelson, *et al.* 2002, ApJ, 568, 610
[12] R. Edelson and J. Krolik. 1988, ApJ, 333, 646
[13] K. Nilsson, *et al.* 2007, A&A, 475, 199
[14] T. Kneiske, *et al.* 2004, A&A, 413, 807
[15] F. Tavecchio, *et al.* 1998, ApJ, 509, 608